Article

Not peer-reviewed version

In-Situ Growth of Fe3N Nanoparticles Encapsulated N-Doped Carbon Nanotubes on Biomass-Derived Carbon Cloth as Self-Standing Electrocatalyst for Oxygen Reduction Reaction

Yongxin Zhao , Dandan Liu , Yubin Tian , Yuzhu Zhai , Chaofan Tian , Sen Li , Tao Xing , Zhi Li , Pengcheng Dai *

Posted Date: 27 July 2023

doi: 10.20944/preprints202307.1854.v1

Keywords: Fe3N nanoparticles; Carbon nanotubes; Biomass; Oxygen reduction reaction; Zn–air battery

Article

In-Situ Growth of Fe_3N Nanoparticles Encapsulated N-Doped Carbon Nanotubes on Biomass-Derived Carbon Cloth as Self-Standing Electrocatalyst for Oxygen Reduction Reaction

Yongxin Zhao [1], Dandan Liu [1], Yubin Tian [1], Yuzhu Zhai [2], Chaofan Tian [1], Sen Li [1], Tao Xing [3], Zhi Li [3,4] and Pengcheng Dai [1,*]

[1] College of New Energy, China University of Petroleum (East China), Qingdao, 266580, China.
[2] College of Textile and Clothing, State Key Laboratory of Bio-Fibers and Eco-Textiles, Collaborative Innovation Center for Eco-textiles of Shandong Province, Qingdao University, Qingdao, 266101, China
[3] New Energy Division, National Engineering Research Center of Coal Gasification and Coal-based Advanced Materials, Shandong Energy Group Co., Ltd., Jining, 273500, China.
[4] School of Materials Science and Engineering, Xi'an Jiaotong University, Xi'an, 710049, China.
* Correspondence: dpcapple@upc.edu.cn

Abstract: The design and fabrication of low-cost catalysts for highly efficient oxygen reduction is of paramount importance for various renewable energy-related technologies, such as fuel cells and metal-air batteries. Herein, we report the in situ growth of Fe3N nanoparticles encapsulated N-doped carbon nanotubes on the surface of flexible biomass-derived carbon cloth (Fe_3N@CNTs/CC) via a simple one-step carbonization process. Taking advantage of its unique structure, Fe_3N@CNTs/CC was employed as a self-standing electrocatalyst for oxygen reduction reaction (ORR) and possessed high activity as well as excellent long-term stability and methanol resistance in alkaline media. Remarkably, Fe_3N@CNT/CC can directly play the role of both gas diffusion layer and electrocatalytic cathode in a zinc-air battery without additional means of catalyst loading, and display higher open circuit voltage, power density, and specific capacity in comparison with the commercial Pt/C catalyst. This work is anticipated to inspire the design of cost-effective, easy-preparation, and high-performance air electrodes for advanced electrochemical applications.

Keywords: Fe_3N nanoparticles; carbon nanotubes; biomass; oxygen reduction reaction; Zn−air battery

1. Introduction

The electrochemical oxygen reduction reaction (ORR) is a critical process in the air electrode in fuel cells and metal-air batteries [1, 2]. It determines the overall chemical-electricity conversion efficiency of these electrochemical devices due to the complicated $4e^-$ reaction pathways, sluggish reaction kinetics, and high overpotential [3]. Platinum (Pt)-based composite materials, due to their high catalytic activity, are commonly recognized as state-of-the-art ORR electrocatalysts. However, their large-scale applications have been severely hindered by solemn drawbacks such as scarce reserves, prohibitive costs, insufficient long-term durability, and vulnerability to methanol crossover [4]. Consequently, considerable efforts have been devoted to developing cost-effective electrocatalysts with competitive activity and excellent stability toward Pt-based materials.

Iron nitrides with rich N content in carbon matrix (Fe_xN-C) with active Fe-N-C sites, as a kind of newly developed non-noble metal electrocatalysts, present enhanced catalytic activity, low cost, and strong methanol tolerance, and have been recognized as promising alternatives to Pt-based catalysts [5, 6]. However, the Fe_xN nanoparticles are thermodynamically unstable and prone to migration and coalescence during the catalysis process because of their high surface energy, resulting in an apparent decrease in activity and stability [7]. Encapsulating the Fe_xN nanoparticles in the nanoshells or nanopores of the carbon matrix is one of the most promising strategies to overcome the stability issue

 doi:10.20944/preprints202307.1854.v1

and benefit the generation of the Fe-N-C active site [8]. Moreover, the FexN-C catalysts are generally connected to the gas diffusion layer to fabricate a gas electrode with ionomers such as Nafion. Li et al. recently found that the Nafion ionomer can be easily deactivated by the generating ·OH radicals, leading to fast performance degradation [9]. By comprehensively evaluating costs, activity, and stability, developing an in-situ growth strategy of Fe_xN nanoparticles encapsulated carbon nanomaterials on gas diffusion electrodes (i.e., carbon cloth) is highly desirable, yet few researchers have been focused on this direction.

In this study, we report that Fe_3N nanoparticles encapsulated N-doped carbon nanotubes in-situ grown on the surface of flexible carbon cloth (denoted as Fe_3N@CNTs/CC) can be synthesized via simple one-step calcination of cotton cloth, one of the most commonly used biomass products. The Fe_3N nanoparticles were produced during the carbonization process of cotton cloth under an ammonia (NH_3) atmosphere and catalyzed the in-situ growth of N-doped carbon nanotubes on the generated carbon cloth, resulting in the overall fabrication of Fe_3N@CNTs/CC hierarchical structure. The hierarchical structure is capable of enlarging the surface area, promotes the exposure of the active species, and gives rise to a remarkable ORR activity with a +50 mV higher half-wave potential ($E_{1/2}$ = 0.91 V) than Pt/C ($E_{1/2}$ = 0.86 V) in alkaline media. The long-term stability and methanol tolerance of Fe_3N@CNTs/CC are also significantly improved compared to Pt/C. Meanwhile, as a flexible and free-standing electrocatalyst, Fe_3N@CNTs/CC can be used directly as the air cathode for Zn-air batteries (ZIBs) and exhibits higher open circuit voltage (1.50 V vs. 1.42 V), power density (157 mW cm^{-2} vs. 124.5 mW cm^{-2}) and specific capacity (814.9 mA h g^{-1} vs. 743.9 mA h g^{-1}) than the Pt/C based gas electrode.

2. Materials and Methods

2.1. Materials and Chemicals

Ferric chloride hexahydrate (analytical pure), zinc acetate dihydrate ⩾ 98%, potassium hydroxide (analytical pure), concentrated sulfuric acid 98%, ethanol 99% purchased from Sinopsin Group Chemical Reagent Co., LTD. Commercial Pt/C catalyst (20 wt%) from Sigma-Aldrich (China), Nafion solution (5%) and Teflon dispersion (60%) from Dupont (USA), Vulcan XC 72R (99.9%) from Johnson Matthey. Deionized water is made in the laboratory.

2.2. Preparation of Fe_3N@CNT/CC

Cellulose cotton cloth (5g) was washed with deionized water thrice and dried in an oven at 80 °C. Next, an impregnation solution was prepared by dissolving 2.7g $FeCl_3 \bullet 6H_2O$ in 5 ml deionized water at 60 °C. The impregnation solution was then dropped evenly onto the cellulose cotton cloth and dried at 80 °C. The impregnated cotton cloth was then annealed in a tube furnace at 1000 °C for 1 hour in an NH_3 atmosphere.

2.3. Physicochemical Characterization

Material Characterization. X-ray diffractometer (XRD, χPert Pro, Panaco, Netherlands) was used to characterize the phase composition of the samples. Field emission scanning electron microscope (SEM, JEOL JSM-7500F) and transmission electron microscope (TEM, JEM 2100F) were used to observe the surface morphology of the materials, and energy-dispersive X-ray spectroscopy (EDS) measurements were performed on an FEI Tecni G20 (USA) transmission electron microscope. X-ray photoelectron spectroscopy (XPS) was used to characterize the material's composition, element content, and valence state. The pore structure and specific surface area of the materials were characterized by N_2 adsorption−desorption isotherms (Quantachrome, USA Autosorb-iQ2) at 77 K. The pore-size-distribution plot was measured by Barrett Joyner-Halenda (BJH) model.

Preprints (www.preprints.org) | NOT PEER-REVIEWED | Posted: 27 July 2023 doi:10.20944/preprints202307.1854.v1

2.4. Electrochemical Measurements

The electrochemical measurements were conducted using a typical three-electrode system of CHI760E electrochemical workstation with 0.1 M KOH as the electrolyte at 25 °C. The platinum wire and Ag/AgCl electrodes were used as the opposite and reference electrodes, respectively. The catalyst-modified glassy carbon rotating disk electrode (RDE) was used as the working electrode (0.1256 cm^2). To prepare the catalyst ink,4 mg catalyst is mixed with 500 μL complex solvent (The volume ratio of ethanol: deionized water: Nafion=9:36:5) and ultrasound for 30 min. The prepared 10 μL catalyst ink droplet was deposited on the turntable electrode (RDE) with a catalyst load of 0.31 mg cm^{-2}.

During the test, cyclic voltammetry (CV) was tested in 0.1 M KOH solution saturated with O_2 or N_2 at a scan rate of 10 mV s^{-1}. Linear sweep voltammetry (LSV) was tested in 0.1 M KOH solution saturated with O_2 or N_2 at a scan rate of 5mV s^{-1}.

The ORR kinetic currents and number of transferred electrons were calculated by the K-L equations:

$$j^{-1} = j_K^{-1} + (j_d)^{-1} = j_K^{-1} + (B\omega^{0.5})^{-1} \quad (1)$$

$$B = 0.2nFC_0D_0^{2/3}\nu^{-1/6} \quad (2)$$

where j is the measured current density (j), j_K is the kinetic current and j_d is diffusion-limiting current, ω is a rotating speed (revolutions per minute), n is the number of transferred electrons, F is the Faraday constant (96,485 C mol^{-1}), C_0 is the bulk concentration of O_2 (1.2×10^{-6} mol cm^{-3}), D_0 is the diffusion coefficient of O_2 ($1.9 \times 10{-}5$ cm^2 s^{-1}), and ν is the kinetic viscosity (0.01 cm^2 s^{-1}).

In the rotating ring disk electrode (RRDE) test, the measured values of the ring and disk currents were used to calculate the H_2O_2 production and the number of electron transfers (n) using the following equation:

$$Y_{H2O2} = 2\times(I_r/N)/(I_d+I_r/N)\times 100\% \quad (3)$$

$$n = 4I_d/(I_d+I_r/N) \quad (4)$$

where I_d denotes the disk current; I_r represents the ring current; N is the current collection efficiency of the Pt ring with a value of 0.36 from the reduction of $K_3[Fe(CN)_6]$. LSV measurements through RRDE tests were carried out at a rotating rate of 1600 rpm and a scan speed of 5 mV s^{-1}. Chronoamperometry was conducted at 0.6 V (vs. RHE) for 10,000 s (1600 rpm) in O_2-saturated 0.1 M KOH to investigate the durability of the catalyst[10].

2.5. Zn–air battery tests

Zn sheet polished with sandpaper was used as the anode. Fe_3N@CNT/CC was applied as the air cathode. The aqueous electrolyte comprised 6 M KOH and 0.2 M zinc acetate. For comparison, Pt/C based air electrode was prepared as follows: 1 mg Pt/C catalyst, 400 μL anhydrous ethanol, and 10 μL Nafion were mixed evenly and then deposited on commercial carbon cloth with a Pt/C loading mass of 0.82 mg cm^{-2}.

3. Results and discussion

3.1. Structural and Compositional Analyses

Fe3N@CNT/CC was prepared by a simple thermal treatment of $FeCl_3$ decorated cellulose cotton cloth in an NH_3 atmosphere, as is illustrated in Figure 1a. The digital images of the Fe_3N@CNT/CC film in Figure 1b reveal its excellent flexibility, as it can be bent and rolled without structural deterioration. SEM analyzed the morphology of Fe3N@CNT/CC. It is observed that the fiber-braided structure of the cotton cloth is well retained during the carbonization process(Figure 1c). Carbon nanotubes are generated and connected to the fibers (Figure 1d) with a diameter of ~100 nm (Figure 1e). Shiny nanoparticles are observed to be encapsulated within the carbon nanotubes (Figure 1e). As is shown in the TEM images (Figure 1f), the nanoparticles have a width of 50-60 nm and a length in

Preprints (www.preprints.org) | NOT PEER-REVIEWED | Posted: 27 July 2023 doi:10.20944/preprints202307.1854.v1

the range of 100-120 nm. The lattice spacing of the nanoparticles is 0.206 nm (Figure 1g), corresponding to the (-1-11) crystal plane of Fe_3N [10, 11]. Additionally, clear lattice fringes are observed outside the nanoparticles with a lattice spacing of 0.34 nm, corresponding to the (002) crystal plane of graphite carbon. The elemental mapping reveals that C and N are evenly distributed throughout the carbon nanotubes, forming N-doped carbon nanotubes. In contrast, Fe was only distributed in the cores of the carbon nanotubes (Figure 1h), indicating Fe_3N nanoparticles are encapsulated in the carbon nanotubes. In this manner, Fe_3N nanoparticles are trapped in the nanocavity of carbon nanotubes, preventing catalyst agglomeration [12].

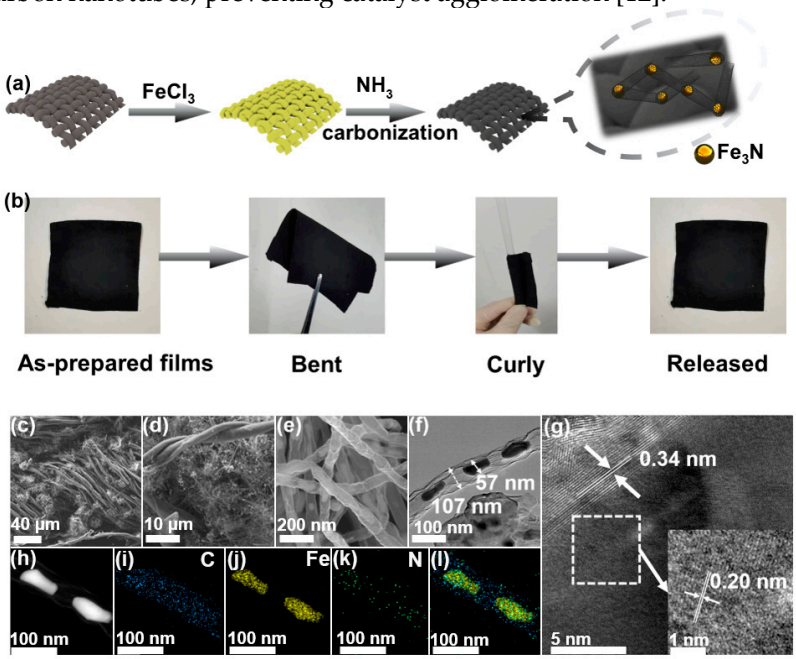

Figure 1. (a) Illustration of the synthetic process of Fe_3N@CNT/CC. (b) Digital photos showing the flexibility of Fe_3N@CNT/CC. (c)-(e) SEM images, (f) TEM image, (g) HRTEM image, and (h)-(l) TEM selective area and its corresponding EDS elemental mappings of Fe_3N@CNT/CC.

X-ray diffraction (XRD) spectrum was recorded to analyze the crystallinity of the obtained Fe_3N@CNT/CC (Figure 2a). The diffraction peaks at 38.2°, 41.1°, 43.6°, 57.3°, 69°, and 76.5°correspond to the (110), (002), (-1-11), (-1-12), (300), and (-1-13) crystal planes of Fe_3N, respectively[3]. The diffraction peak at 26.4° corresponds to the (002) facet of graphite carbon[3], consistent with the HRTEM results. Figure 2b depicts the Raman spectrogram analysis of the Fe_3N@CNT/CC, which exhibits two distinct peaks at 1344 cm^{-1} and 1574 cm^{-1}, corresponding to the typical D and G bands of carbon materials[13]. The ratio of I_D/I_G indicates the degree of defect of the carbon material[14]. The I_D/I_G value of Fe_3N@CNT/CC is determined to be about 0.89, which suggests that less defective or amorphous carbon exists in the as-prepared product. Nitrogen adsorption and desorption isotherm reveal that Fe_3N@CNT/CC possesses a specific surface area of 337.7 $m^2 \cdot g^{-1}$ (Figure 2c). The pore volume is mainly contributed by the micropore, while a certain amount of mesopores also exist with an average size of 4 nm (Figure 2d). The high surface area and pore volume can make the catalytically active sites accessible and ensure fast mass transport efficiency, which enables the catalyst to have significant advantages in electrocatalytic reactions[15, 16].

Preprints (www.preprints.org) | NOT PEER-REVIEWED | Posted: 27 July 2023 doi:10.20944/preprints202307.1854.v1

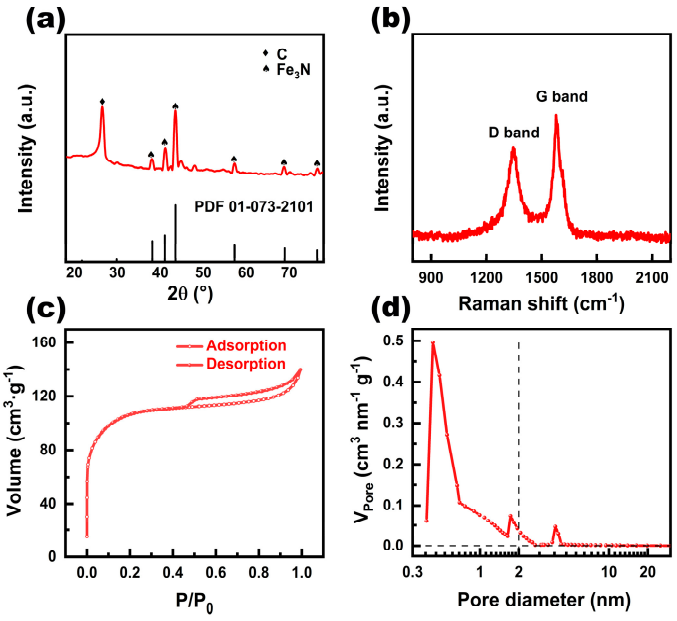

Figure 2. (a) XRD pattern, (b) Raman spectrum, (c) Nitrogen adsorption and desorption isotherm, and (d) the pore size distribution of Fe_3N@CNT/CC.

The XPS survey spectrum (Figure 3a) reveals the presence of C, N, Fe, and O. In the C 1s spectrum (Figure 3b), the peaks at 284.8 eV, 285.5 eV, and 287.8 eV correspond to C-C, C-N, and C-O signals, respectively [17]. The N 1s (Figure 3c) spectrum is divided into four peaks, including pyridinic nitrogen (398.2 eV), Fe-Nx (399.4 eV), pyrrolic nitrogen (401 eV), and graphite nitrogen (402.1 eV)[18]. The peak corresponding to Fe-N bond can be observed at 707.8eV[19] in the Fe 2p spectrum (Figure 3d). The existence of C-N in the C 1s spectrum, Fe-Nx in the N 1s spectrum, and the Fe-N bond in the Fe 2p spectrum verify the formation of Fe-N-C sites, which has been proved to be an efficient ORR active sites[20]. Meanwhile, the graphitized N-doped carbon promotes the electron transfer process, further improving the electrical conductivity of the sample. [3]

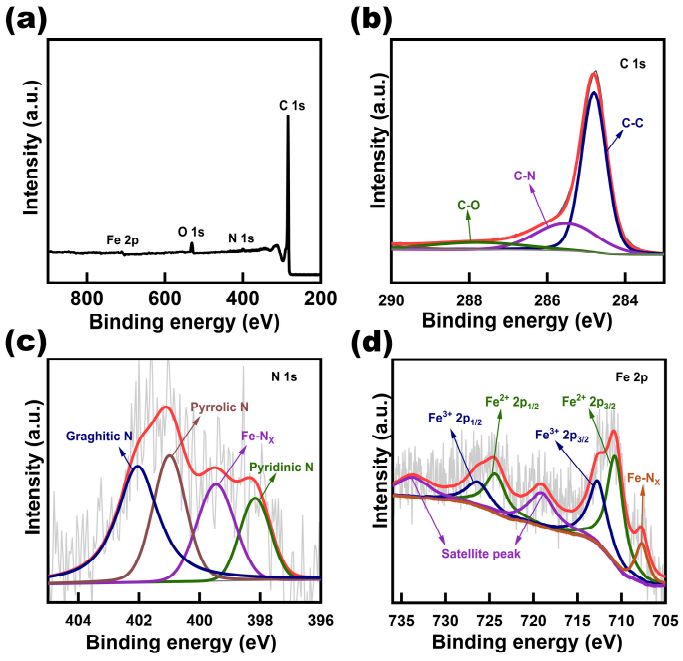

Figure 3. (a) XPS survey spectrum, (b) High-resolution C 1s, (c) High-resolution N 1s, and (d) High-resolution Fe 2p spectrum of Fe_3N@CNT/CC.

3.2. Electrocatalytic Activities of Fe_3N@CNT/CC for ORR

The ORR performances of Fe_3N@CNT/CC are compared with commercial Pt/C (Figure 4). Fe_3N@CNT/CC demonstrated no ORR peaks in N_2-saturated electrolyte, while distinguished reduction peak for ORR appeared when the electrolyte was saturated with O_2 (Figure 4a). The peak potentials corresponding to Fe_3N@CNT/CC was 0.91V, 60 mV positive than that corresponding to 20% Pt/C (0.85 V) (Figure 4a, Figure S1). The LSV curve of Fe_3N@CNT/CC (Figure 4b) shows an onset potential of 1.0 V, a half-wave potential of 0.91 V, and a limit current density of 5.6 $mA \cdot cm^{-1}$. In contrast, the initial potential (0.9 V), half-wave potential (0.86 V), and limit current (5 $mA \cdot cm^{-1}$) of Pt/C catalyst were significantly worse than those of Fe_3N@CNT/CC. The corresponding Tafel slope of Fe_3N@CNT/CC (Figure 4c) was 78 $mV \cdot dec^{-1}$, lower than that of Pt/C (88 $mV \cdot dec^{-1}$), indicating that Fe_3N@CNT/CC had a faster catalytic kinetic process[3].

The ORR reactions have two types of electron transfer processes: $2e^-$ transfer process and $4e^-$ transfer process. In the $2e^-$ transfer process, oxygen reacts to produce H_2O_2 through the catalytic process[21]. The reaction rate of this process is slow, which is not suitable for application in zinc-air batteries[22]. Moreover, the generated H_2O_2 can cause damage to catalyst and battery components[23, 24]. The catalytic product of the $4e^-$ transfer process is H_2O, making it the required catalytic path for the ORR catalytic reaction[25]. The number of transferred electrons (n) in the catalytic reactions was obtained by the Koutecký-Levich (K-L) calculation of the LSV curves at different speeds (Figure 4d). As is shown in Figure 4e, the average number of transferred electrons of Fe_3N@CNT/CC was determined to be 3.99, which is close to the theoretical value of 4 and comparable to that of Pt/C. In addition, rotating ring-disk electrode (RRDE) measurements were conducted to explore the ORR pathway of Fe_3N@CNT/CC (Figure S2). The H_2O_2 yield of Fe_3N@CNT/CC was found to be only 0.14%–0.01% from 0.2 V to 0.8 V (Figure 4f), further proving the 4- electron transfer process.

Subsequently, the stability of Fe_3N@CNT/CC and Pt/C catalyst was assessed using timed amperometry at 0.8 V (vs. RHE). The current retention of Fe_3N@CNT/CC decreased by 2.75% during the test at 10000 s, whereas that of the Pt/C decreased by 16.5% (Figure 4g). It was observed that Fe_3N@CNT/CC is more stable during the reaction. Figure 4h depicts the durability test of Fe_3N@CNT/CC after 2000 CV cycle curves. It can be observed that the half-wave potential value of the catalyst only decreased by 20 mV after 2000 accelerated aging experiments, indicating its excellent stability as well. Methanol resistance is another essential index in ORR. It is seen from Fig.S3 that when methanol was added to the electrolyte, the current value of Fe_3N@CNT/CC decreased by 5%, whereas the current density of Pt/C decreased by 35% (Figure S3), which suggests that Fe_3N@CNT/CC exhibits outstanding resistance to methanol.

Preprints (www.preprints.org) | NOT PEER-REVIEWED | Posted: 27 July 2023 doi:10.20944/preprints202307.1854.v1

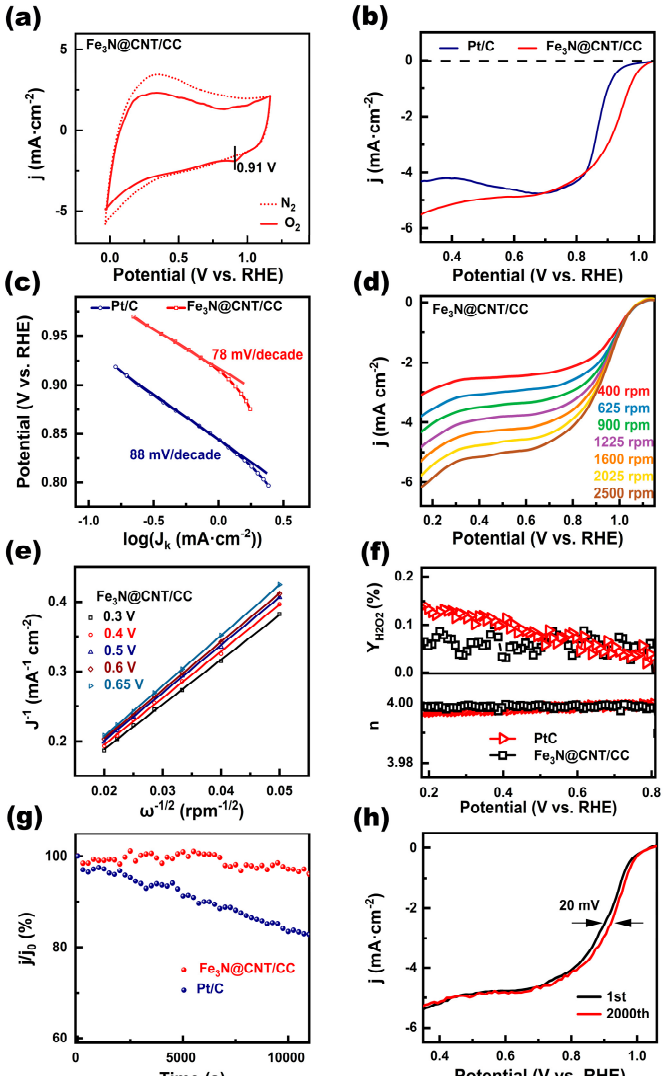

Figure 4. (a) CV curves of the Fe_3N@CNT/CC in N_2 (dotted line) and O_2 (solid line) saturated 0.1 M KOH electrolyte with a scan rate of 10 mV·s^{-1}, (b) LSV curves of the Fe_3N@CNT/CC and Pt/C, (c) The corresponding Tafel plots and slops, (d) LSV curves of Fe_3N@CNT/CC at different speeds, (e) K-L plot of Fe_3N@CNT/CC, (f) Electron transfer number and H_2O_2 yield of Fe_3N@CNT/CC and Pt/C, (g)Long-term stability test of Fe_3N@CNT/CC and Pt/C, (h) Durability measurement of Fe_3N@CNT/CC.

3.3. Application of Fe_3N@CNT/CC Catalyst in ZAB

To further evaluate the practical application of Fe_3N@CNT/CC, it is essential to assemble it as the air cathode of a ZAB, as illustrated in Figure 5a. The open circuit voltage of the carbon cloth composed of Fe_3N@CNT/CC is approximately 1.5 V (Figure 5b), which is higher than that of Pt/C (1.43 V). As shown in Figure 5c, Fe_3N@CNT/CC can supply a higher voltage at the same current density than Pt/C. The peak discharge power density of the ZAB with Fe_3N@CNT/CC as the air cathode is 157 mW cm^{-2} at the current density of 300 mA cm^{-2}(Figure 5c, 5d), which is higher than that of the Pt/C (124.5 mW cm^{-2}). Figure 4e illustrates the constant current discharge test of the battery at a current density of 10 mA cm^{-2}. The specific capacity of Fe_3N@CNT/CC-based ZAB is 814.9 mAh g^{-1}, also higher than that of the Pt/C (737.9 mAh g^{-1}). In addition, Figure 5f depicts the cycling stability of Fe_3N@CNT/CC-based ZAB. The voltage range does not widen during the 100-hour charge-discharge cycle, indicating the catalyst has excellent stability.

Preprints (www.preprints.org) | NOT PEER-REVIEWED | Posted: 27 July 2023 doi:10.20944/preprints202307.1854.v1

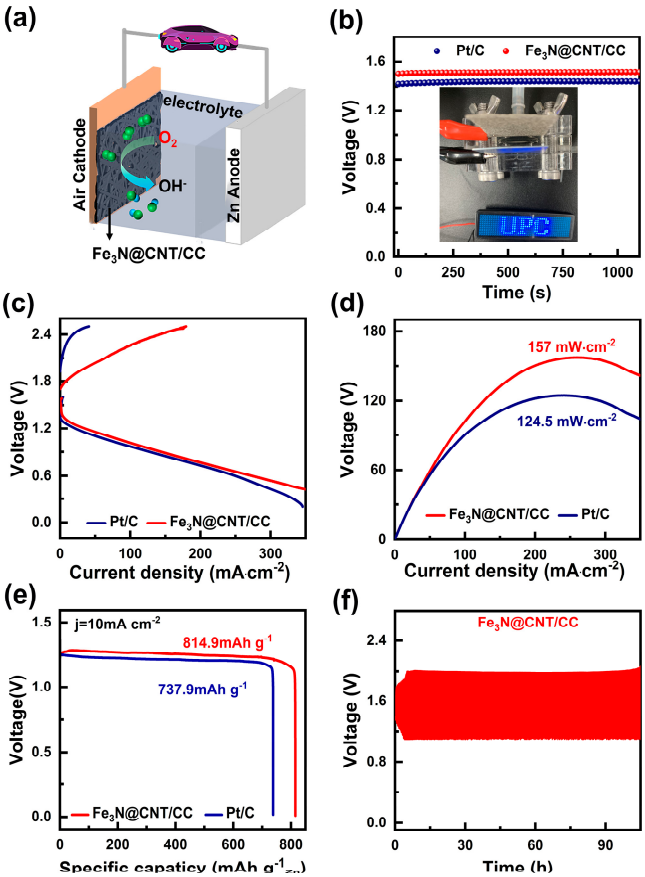

Figure 5. (a) Schematic of the as-assembled zinc-air battery, (b) Open circuit voltage, (c) polarization curves, (d) power density curves of the ZABs assembled with Fe_3N@CNT/CC and Pt/C, (e) The discharge specific capacity curves of the ZAB with Fe_3N@CNT/CC and Pt/C at a current density of 10 mA cm^{-2}, (f)the cycling stability of Fe_3N@CNT/CC-based ZAB.

4. Conclusions

In this work, Fe_3N nanoparticles encapsulated N-doped carbon nanotubes grown on the surface of flexible carbon cloth were synthesized via simple one-step calcination of cotton cloth. The structure feather and ORR performance of as-prepared catalysts were investigated in detail. The hierarchical structure can stable the active sites, promote the exposure of the active species, and possess satisfactory ORR performance, including excellent half-wave potential, higher long-term stability, and satisfactory resistance to methanol, overtopping commercial Pt/C catalysts. Benefiting from the unique structure, Fe_3N@CNTs/CC can be used directly as a free-standing air cathode for ZABs, exhibiting higher open circuit voltage, power density, and specific capacity than the Pt/C-based gas electrode. This work paves the way for the construction of cost-effective, easy-preparation, and high-performance ORR catalysts and ZAB energy conversion devices.

Supplementary Materials: The following supporting information can be downloaded at: www.mdpi.com/xxx/s1. Figure S1: CV curves of the Pt/C in N_2 and O_2 saturated 0.1 M KOH electrolyte with a scan rate of 10 mV·s^{-1}. Figure S2: RRDE voltammograms of Fe_3N@CNT/CC at a rotation rate of 1600 rpm; Figure S3: The chronoamperometric curves of Fe_3N@CNT/CC and Pt/C acquired by injecting 1.0 M methanol at 100 s.

Author Contributions: Conceptualization, D.L. and P.D.; methodology,Y.T.; validation, D.L.; formal analysis, C.T.; data curation, S.L.; writing—original draft preparation, Y.Z.; writing—review and editing, Y.Z.; visualization, Y.Z.; supervision, P.D.; funding acquisition, T.X. and Z.L. All authors have read and agreed to the published version of the manuscript. Y.Z. and D.L. contributed equally to this work.

Funding: This research was funded by the National Natural Science Foundation of China (51702365), the Natural Science Foundation of Shandong Province (ZR2022MB133), KeyResearch and Development Plan of Shandong

Province (2019GGX102056, 2018GGX104018), New Faculty Start-up funding in China University of Petroleum (East China) (YJ201501029).

Conflicts of Interest: The authors declare no conflict of interest.

References

1. Nie, Y.; Xu, X.; Wang, X.; Liu, M.; Gao, T.; Liu, B.; Li, L.; Meng, X.; Gu, P.; Zou, J. Coni alloys encapsulated in n-doped carbon nanotubes for stabilizing oxygen electrocatalysis in zinc-air battery. *Nanomaterials*. **2023**, *13*, 1788.
2. Cebollada, J.; Sebastián, D.; Lázaro, M. J.; Martínez-Huerta, M. V. Carbonized polydopamine-based nanocomposites: The effect of transition metals on the oxygen electrocatalytic activity. *Nanomaterials*. **2023**, *13*, 1549.
3. Li, T.; Li, M.; Zhang, M.; Li, X.; Liu, K.; Zhang, M.; Liu, X.; Sun, D.; Xu, L.; Zhang, Y.; Tang, Y. Immobilization of fe3n nanoparticles within n-doped carbon nanosheet frameworks as a high-efficiency electrocatalyst for oxygen reduction reaction in zn-air batteries. *Carbon*. **2019**, *153*, 364-371.
4. Yu, X.; Ye, S. Recent advances in activity and durability enhancement of pt/c catalytic cathode in pemfc : Part ii: Degradation mechanism and durability enhancement of carbon supported platinum catalyst. *Journal of Power Sources*. **2007**, *172*, 133-144.
5. Yang, W.; Chen, L.; Liu, X.; Jia, J.; Guo, S. A new method for developing defect-rich graphene nanoribbons/onion-like carbon@co nanoparticles hybrid materials as an excellent catalyst for oxygen reactions. *Nanoscale*. **2017**, *9*, 1738-1744.
6. Xiao, J.; Xu, Y.; Xia, Y.; Xi, J.; Wang, S. Ultra-small fe2n nanocrystals embedded into mesoporous nitrogen-doped graphitic carbon spheres as a highly active, stable, and methanol-tolerant electrocatalyst for the oxygen reduction reaction. *Nano Energy*. **2016**, *24*, 121-129.
7. Ma, Q.; Jin, H.; Zhu, J.; Li, Z.; Xu, H.; Liu, B.; Zhang, Z.; Ma, J.; Mu, S. Stabilizing fe–n–c catalysts as model for oxygen reduction reaction. *Advanced Science*. **2021**, *8*, 2102209.
8. Li, Z.; Fang, Y.; Zhang, J.; Lou, X. W. Necklace-like structures composed of fe3n@c yolk–shell particles as an advanced anode for sodium-ion batteries. *Advanced Materials*. **2018**, *30*, 1800525.
9. Zhou, L.; Li, Y.; Chen, X.; Yang, Z.; Yang, S.; Wang, Q.; Liu, X.-Y.; Lu, S. New insights into degradation of fe–n–c catalyst layers: Ionomer decomposition. *Journal of Materials Chemistry A*. **2022**, *10*, 20323-20330.
10. Hu, Y.; Huang, D.; Zhang, J.; Huang, Y.; Balogun, M.-S. J. T.; Tong, Y. Dual doping induced interfacial engineering of fe2n/fe3n hybrids with favorable d-band towards efficient overall water splitting. *ChemCatChem*. **2019**, *11*, 6051-6060.
11. Chen, Z. Y.; Li, Y. N.; Lei, L. L.; Bao, S. J.; Wang, M. Q.; Heng, L.; Zhao, Z. L.; Xu, M. W. Investigation of fe2n@carbon encapsulated in n-doped graphene-like carbon as a catalyst in sustainable zinc–air batteries. *Catalysis Science & Technology*. **2017**, *7*, 5670-5676.
12. Zhang, N.; Xie, S.; Wang, W.; Xie, D.; Zhu, D.; Cheng, F. Ultra-small fe2n/n-cnts as efficient bifunctional catalysts for rechargeable zn-air batteries. *Journal of The Electrochemical Society*. **2020**, *167*, 020505.
13. Compagnini, G.; Puglisi, O.; Foti, G. Raman spectra of virgin and damaged graphite edge planes. *Carbon*. **1997**, *35*, 1793-1797.
14. Li, L.; Qing, M.; Liu, X.; Wang, H.; Liu, S.; Zhang, Y.; Wan, H.; Wen, X.; Yang, Y.; Li, Y. Efficient one-pot synthesis of higher alcohols from syngas catalyzed by iron nitrides. *ChemCatChem*. **2020**, *12*, 1939-1943.
15. Zhu, C.; Fu, S.; Song, J.; Shi, Q.; Su, D.; Engelhard, M. H.; Li, X.; Xiao, D.; Li, D.; Estevez, L.; Du, D.; Lin, Y. Self-assembled fe–n-doped carbon nanotube aerogels with single-atom catalyst feature as high-efficiency oxygen reduction electrocatalysts. *Small*. **2017**, *13*, 1603407.
16. Du, P.; Bao, Y.; Guo, C.; Wu, L.; Pan, J.; Zhao, C.; Ma, F.-X.; Lu, J.; Li, Y. Y. Design of fe,n co-doped multi-walled carbon nanotubes for efficient oxygen reduction. *Chemical Communications*. **2020**, *56*, 14467-14470.
17. Zhu, G.; Ma, L.; Lv, H.; Hu, Y.; Chen, T.; Chen, R.; Liang, J.; Wang, X.; Wang, Y.; Yan, C.; Tie, Z.; Jin, Z.; Liu, J. Pine needle-derived microporous nitrogen-doped carbon frameworks exhibit high performances in electrocatalytic hydrogen evolution reaction and supercapacitors. *Nanoscale*. **2017**, *9*, 1237-1243.

18. Guo, C.; Li, L.; Zhang, T.; Xu, Y.; Huo, Y.; Li, S. Space-confined iron nanoparticles in a 3d nitrogen-doped rgo-cnt framework as efficient bifunctional electrocatalysts for rechargeable zinc–air batteries. *Microporous and Mesoporous Materials*. **2020**, *298*, 110100.
19. Liu, S.; Zheng, W.; Xie, W.; Cui, H.; Li, Y.; Zhang, C.; Ji, Z.; Liu, F.; Chen, R.; Sun, H.; Xu, J. Synthesis of three-dimensional honeycomb-like fe3n@nc composites with enhanced lithium storage properties. *Carbon*. **2022**, *192*, 162-169.
20. Ma, J.; Li, J.; Wang, R.; Yang, Y.; Yin, P.; Mao, J.; Ling, T.; Qiao, S. Hierarchical porous s-doped fe–n–c electrocatalyst for high-power-density zinc–air battery. *Materials Today Energy*. **2021**, *19*, 100624.
21. Zhou, X.; Gao, J.; Hu, Y.; Jin, Z.; Hu, K.; Reddy, K. M.; Yuan, Q.; Lin, X.; Qiu, H.-J. Theoretically revealed and experimentally demonstrated synergistic electronic interaction of cofe dual-metal sites on n-doped carbon for boosting both oxygen reduction and evolution reactions. *Nano Letters*. **2022**, *22*, 3392-3399.
22. Wang, B.; Tang, J.; Zhang, X.; Hong, M.; Yang, H.; Guo, X.; Xue, S.; Du, C.; Liu, Z.; Chen, J. Nitrogen doped porous carbon polyhedral supported fe and ni dual-metal single-atomic catalysts: Template-free and metal ligand-free sysnthesis with microwave-assistance and d-band center modulating for boosted orr catalysis in zinc-air batteries. *Chemical Engineering Journal*. **2022**, *437*, 135295.
23. Ye, H.; Li, L.; Liu, D.; Fu, Q.; Zhang, F.; Dai, P.; Gu, X.; Zhao, X. Sustained-release method for the directed synthesis of zif-derived ultrafine co-n-c orr catalysts with embedded co quantum dots. *ACS Applied Materials & Interfaces*. **2020**, *12*, 57847-57858.
24. Hu, C.; Dai, L. Carbon-based metal-free catalysts for electrocatalysis beyond the orr. *Angewandte Chemie International Edition*. **2016**, *55*, 11736-11758.
25. Zhang, J.; Wang, M.; Wan, T.; Shi, H.; Lv, A.; Xiao, W.; Jiao, S. Novel (pt-o(x))-(co-o(y)) nonbonding active structures on defective carbon from oxygen-rich coal tar pitch for efficient her and orr. *Adv Mater*. **2022**, *34*, e2206960.